Adaptive damage localization based on locally perturbed dynamic equilibrium and hierarchical clustering

Shancheng Cao[1,2], Huajiang Ouyang[3] and Li Cheng[1,2,*]

[1]Department of Mechanical Engineering, The Hong Kong Polytechnic University, Kowloon, Hong Kong, China

[2]Hong Kong Branch of National Rail Transit Electrification and Automation Engineering Technology Research Centre, The Hong Kong Polytechnic University, Hung Hom, Hong Kong

[3]Department of Mechanical, Materials and Aerospace Engineering, School of Engineering, The University of Liverpool, Liverpool, L69 3GH, U.K.

Abstract

Pseudo-excitation (PE) method is a recently developed damage identification method for flexible structures containing components like beams, plates and shells. Characterized by the high-order spatial derivatives, the approach has been shown to feature a high sensitivity to local damage. However, two major issues, *i.e.* susceptibility to measurement noise and unknown material/structural properties, hamper its practical applications. To tackle these problems, an adaptive damage localization method is proposed for plate-type structures, which combines the PE method with hierarchical clustering. In the proposed method, a general dynamic equilibrium model, involving unknown material/structural properties, is statistically identified and further used for damage localization. Moreover, noise-induced effects are quantified by using a hierarchical clustering for performance assessment of damage localization and process optimization of spatial derivative estimation to achieve more accurate damage localization. Meanwhile, a data fusion scheme is developed to avoid blind inspection zones, thus enhancing the capability of damage localization. Both numerical and experimental studies of cantilever plates containing two damage zones are conducted to validate the feasibility and the effectiveness of the proposed adaptive damage localization method. Results demonstrate that the proposed method outperforms the traditional PE method in terms of

* Corresponding author, email address: li.cheng@polyu.edu.hk

detection accuracy and robustness.

Keywords: damage localization, local dynamic equilibrium, pseudo-excitation, spatial derivatives, hierarchical clustering

1 Introduction

Vibration-based damage identification plays an important role in structural health monitoring and has experienced a rapid development in the past several decades [1-4]. The basic principle of vibration-based techniques consists in examining damage-induced changes in the vibration signatures under various operational and environmental conditions [5-9]. Generally speaking, vibration-based damage identification methods can be categorized according to different criteria such as the damage identification level, linear or nonlinear vibration responses and whether physics-based models are used or not [10-15]. Recently, a novel damage identification approach, referred to as pseudo-excitation (PE) method, was proposed for damage identification in beam-, plate- and shell-type structures by examining the damage-induced perturbation in the dynamic equation of local structural components [16, 17].

The fundamental idea behind the PE method originates from the local force identification problem [18, 19]. As for damage identification, the construction of a damage index for a damaged structure can be equivalently treated as the identification of pseudo-excitation forces on its intact counterpart [20, 21]. Naturally, damage alters the local structural properties like cross-section area or Young's modulus, which in turn alters the local dynamic equilibrium [22-24]. Consequently, the peak/sudden changes in the reconstructed force distribution along the structure (in spatial domain) can be used to pinpoint the presence, locations or the size of the damage [25].

PE method has several advantages over some traditional vibration-based methods [26, 27]. Firstly, structural damage is identified by using the measured displacement of damaged structures without requiring the baseline data on pristine structures or benchmark structures. Secondly, spatially distributed local information along the structures is used, which is more sensitive to local damage than the global damage feature-based methods. Furthermore, it examines the inspection region point-by-point without requiring the global model of the entire structure. Thus, the method is applicable to

multi-damage detection. In addition, due to its local feature, structural boundary conditions have no effects and the method is immune from environmental variability such as changes of temperature and humidity.

However, the damage localization index used in the PE approach is based on the equation of local motion, thus inheriting two major drawbacks. Firstly, the calculation of the high-order spatial derivatives of the displacement is highly sensitive to the measurement noise, since the finite difference method, usually adopted for spatial derivative estimation, severely propagates and amplifies the effects of measurement noise [28, 29]. Secondly, some material/structural parameters in the equation of local motion such as Young's modulus, Poisson's ratio and damping may be inaccurately described or even unknown *a priori* [30].

Traditionally, denoising techniques, exemplified by wavelet analysis [23, 31, 32] and wavenumber filtering [16, 26, 33], have been widely used to enhance the estimation accuracy of displacement spatial derivatives. Despite these efforts, two major problems still exist: one being the relationship between the estimation accuracy of the spatial derivatives and the performance of the damage localization, and the other one being the selection of the regularization parameters (such as the scale parameter of wavelet analysis) during spatial derivative estimation for more accurate damage localization. As for structures with unknown material/structural parameters, a general local vibration model without considering the damping effects is typically assumed [30, 34]. As a result, the application of the traditional PE method based on this assumption of no damping is limited to non-resonant frequencies. However, an enhanced PE method based on vibration data under resonant frequencies is more desirable due to the high signal to noise ratio. Moreover, the damage index based on the statistically identified vibration model does not ideally zero for pristine plates due to the measurement noise effects, which may produce misleading damage localization results.

Motivated by overcoming the afore-mentioned problems of the traditional PE method, the present work proposes a comprehensive approach to tackle the aforementioned problems, with the aim of improving the practical applicability of the PE method. Firstly, a novel adaptive damage localization method is proposed to obtain the most accurate damage localization by optimizing the estimate of

high-order spatial derivatives. The proposed approach contains two steps. Firstly, the measurement noise-induced features in the damage index (which is based on the fourth-order spatial derivatives of displacements) are characterized and quantified by using a hierarchical clustering. Secondly, a fully automated framework for high-order spatial derivate estimation is developed to reduce the noise features for better damage localization through a proper tuning of the process. Moreover, a vibration model incorporating viscous damping effects is adopted and statistically identified to construct the damage index, thus extending the applicability of the PE method to both resonant and non-resonant conditions. In addition, a normalization and thresholding process is also proposed to enhance the noise-robustness and the accuracy of the damage index.

The outline of the paper is as follows. An enhanced PE method is first formulated in Section 2, including both damping effects and a data fusion scheme. In Section 3, a general form of the local dynamic equation is constructed for structures with unknown material/structural parameters. In Section 4, a local bivariate polynomial with adaptive selection of the fitting points is then developed for noise-robust fourth-order derivative estimation. The effects of the measurement noise are quantified by using a hierarchical clustering. Numerical and experimental studies are presented for validations in Section 5 and Section 6, respectively. Finally, key conclusions are given in Section 7.

2 Enhanced pseudo-excitation method

In principle, the PE method is applicable to any structural components such as beams, plates and shells as long as the inspected structural component can be locally described by an equation of motion. Without loss of generality, a plate-like component undergoing transverse vibrations is taken as an example, the equation of motion is defined according to the Kirchhoff-Love theory as

$$D\nabla^4 w(x,y,t) + C\frac{\partial w(x,y,t)}{\partial t} + \rho h\frac{\partial^2 w(x,y,t)}{\partial t^2} = f(x,y,t) \qquad (1)$$

where $w(x,y,t)$ and $f(x,y,t)$ are the flexural displacement and transverse force at location (x,y), respectively; $D = Eh^3/[12(1-\upsilon^2)]$ is the plate's flexural rigidity with Young's modulus E, plate thickness h and Poisson's ratio υ. C and ρ are the viscous damping coefficient and mass density, respectively. The operator $\nabla^4 w(x,y,t)$ is defined as

$$\nabla^4\big(w(x,y,t)\big) = \frac{\partial^4 w(x,y,t)}{\partial x^4} + 2\frac{\partial^4 w(x,y,t)}{\partial x^2 \partial y^2} + \frac{\partial^4 w(x,y,t)}{\partial y^4} \qquad (2)$$

Specifically, under harmonic excitation, steady-state vibration $w(x,y,t)$ can be expressed by $W(x,y)$. Assuming that the plate possesses a uniform cross-section and constant material properties within the inspection area, Eq. (1) can be simplified in a harmonic regime as

$$D\nabla^4 W(x,y) + \mathrm{j}C\omega W(x,y) - \rho h\omega^2 W(x,y) = f(x,y,\omega) \tag{3}$$

in which j=$\sqrt{-1}$. In Eq. (3), the left side is identical to zero for a pristine plate, when the external excitation $f(x,y,\omega)$ is absent. However, with the presence of damage in the plate component, the left side of Eq. (3) does not equal zero when $f(x,y,\omega)=0$, which can be taken as an effective damage index (DI) as

$$\begin{aligned} DI(x,y,\omega) = &\left[(D-\Delta_D)\nabla^4 W(x,y) + \mathrm{j}(C-\Delta_c)\omega W(x,y) - \left(\rho h - \Delta_{\rho h}\right)\omega^2 W(x,y)\right] \\ &+\left[\Delta_D\nabla^4 W(x,y) + \mathrm{j}\Delta_c\omega W(x,y) - \Delta_{\rho h}\omega^2 W(x,y)\right] \end{aligned} \tag{4}$$

where Δ_D, Δ_c and $\Delta_{\rho h}$ denote the damage-induced changes in the structural properties associated with its stiffness, damping and mass, respectively. Due to the local dynamic equilibrium, the first term of Eq. (4) equals zero, which is

$$(D-\Delta_D)\nabla^4 W(x,y) + \mathrm{j}(C-\Delta_c)\omega W(x,y) - \left(\rho h - \Delta_{\rho h}\right)\omega^2 W(x,y) = 0 \tag{5}$$

It is seen from Eq. (4) and Eq. (5) that the transverse vibration of a damaged plate component is equivalent to its corresponding pristine counterpart subjected to a virtual excitation force, referred to as pseudo-excitation force (the second term of Eq. (4)). Therefore, the damage induced pseudo-excitation force can be used to detect, localize or even quantify the damage and $DI(x,y,\omega)$ of the damaged component is expressed as

$$DI(x,y,\omega) = \Delta_D\nabla^4 W(x,y) + \mathrm{j}\Delta_c\omega W(x,y) - \Delta_{\rho h}\omega^2 W(x,y) \tag{6}$$

By considering the damping effects in Eq. (6), the proposed DI is applicable to both resonant and non-resonant frequencies. For practical applications, the statistically identified mode shape data of a structure can be used and are preferred to construct the DI in Eq. (6), as the mode shape data can be considered as the normalized displacement data that possess high signal to noise ratio. Moreover, the mode shape data can be readily extracted from acceleration, velocity or displacement measurements.

Naturally, for any given ω, the sensitivity of the $DI(x,y)$ to damage depends on locations [16].

Hence, an enhanced damage index integrating damage-induced characteristics at different frequencies should be more robust and accurate, which is defined as

$$DI(x,y) = \sum_i |DI(x,y,\omega_i)| \tag{7}$$

Having setting up the enhanced PE formalism, two critical issues are to be resolved: unknown material/structural properties and the evaluation of the fourth-order spatial derivatives of $W(x,y)$. These two issues will be addressed in Section 3 and Section 4, respectively.

3 Damage localization with unknown material/structural properties

In practice, the values of D, C and ρh may not be available. Even if they were available, discrepancies between the theoretical and the actual material/structural values would be inevitable. To address this problem, a damage localization strategy is developed, which overcomes the absence of prior knowledge on material properties, geometric parameters and boundary conditions of the inspected structures.

To demonstrate the proposed strategy, Eq. (6) is adopted without loss of generality. In Eq. (6), the basic material properties (ρ, υ, C and E), geometric parameter (h) and boundary conditions are assumed to be unknown *a priori*. Instead of identifying the individual material and geometric parameters, combined parameters are used through casting Eq. (6) into the following form:

$$DI(x,y,\omega) = a_0 \nabla^4 W(x,y) + W(x,y) \tag{8}$$

in which, $a_0 = D/(\mathrm{j}C\omega - \rho h\omega^2)$ is a constant for a given ω. Assuming that each damage zone only occupies a small area of the whole structure, most part of the structure still satisfy $DI(x,y,\omega) = 0$ within the inspection region in the absence of any external excitation. Thus, coefficient a_0 can be effectively evaluated according to the least-squares criterion at each interested angular frequency ω.

However, the constructed $DI(x,y,\omega)$ in Eq. (8) does not ideally equal to zero even within the non-damaged area due to measurement noise. To alleviate this, a normalization and thresholding procedure is harnessed to enhance the estimated $DI(x,y,\omega)$.

First, $DI(x,y,\omega)$ is normalized as

$$DI(x,y,\omega) = \left(DI(x,y,\omega) - \overline{DI}(\omega)\right)/\sigma_{DI(\omega)} \tag{9}$$

where $\overline{DI}(\omega)$ and $\sigma_{DI(\omega)}$ denote the mean value and the standard deviation of all entries in $DI(\omega)$, respectively.

Then, a threshold value is determined according to the three-sigma limits of a normal distribution to reduce the effects of measurement noise. Normally, for a pristine structure, the values of $DI(\omega)$ mostly sit in the range of $\left[\overline{DI}(\omega) - 3\sigma_{DI(\omega)}, \overline{DI}(\omega) + 3\sigma_{DI(\omega)}\right]$ and the outlier values outside this range tend to be scattered over the plate surface. However, the presence of damage will produce more outlier values outside $\left[\overline{DI}(\omega) - 3\sigma_{DI(\omega)}, \overline{DI}(\omega) + 3\sigma_{DI(\omega)}\right]$, which tend to be spatially close to each other around the damage. Therefore, the outlier values located outside the three standard deviations from the mean are taken for damage localization and the enhanced noise-robust $DI(x,y,\omega)$ is expressed as

$$DI(x,y,\omega) = \begin{cases} |DI(x,y,\omega)|, & |DI(x,y,\omega)| \geq \overline{DI}(\omega) + 3\sigma_{DI(\omega)} \\ 0, & |DI(x,y,\omega)| < \overline{DI}(\omega) + 3\sigma_{DI(\omega)} \end{cases} \tag{10}$$

in which $DI(x,y,\omega)$ requires neither baseline data on pristine structures nor the prior knowledge on their material/structural properties.

4 Adaptive damage localization via the fourth-order derivative estimation

To get $DI(x,y,\omega)$ from Eq. (6), $\nabla^4\left(W(x,y)\right)$ is typically evaluated from $W(x,y)$ through a finite difference calculation scheme, which severely amplifies the effects of measurement noise [35]. To overcome this problem, a systematic approach is proposed to achieve the most accurate damage localization by optimizing the estimation of $\nabla^4\left(W(x,y)\right)$. In this method, the performance of damage localization is evaluated and quantified by using hierarchical clustering.

4.1 The fourth-order derivative estimation

The estimation of $\nabla^4\left(W(x,y)\right)$ can be categorized into either discrete or continuous methods [36]. The discrete method applies the direct calculation formula to the discrete representation points of the underlying displacement surface. The continuous method firstly employs a local bivariate polynomial technique to fit the current point and its adjacent measurement points as shown in Eq. (11), and then

evaluates the derivatives based on the fitted local displacement surface [37].

$$\widehat{W}_p(x,y) = \sum_{i_2=0}^{n} \sum_{i_1=0}^{i_2} c_{i_1,i_2-i_1} x^{i_1} y^{i_2-i_1} \tag{11}$$

where $\widehat{W}_p(x,y)$ indicates the fitted displacement value at point p and n denotes the order of the polynomial.

However, the direct application of Eq. (11) for $\nabla^4\big(W(x,y)\big)$ estimation involves several other high-order terms such as x^3, y^3, xy^3 and x^3y. Furthermore, the higher the order of the polynomial in Eq. (11), the more adjacent measurement points are required to evaluate the coefficients. Therefore, in order to avoid the involvement of some useless high-order terms and simplify the calculation process of $\nabla^4\big(W(x,y)\big)$, a double second-order derivative procedure is proposed, expressed as

$$\nabla^4\big(W(x,y)\big) = \nabla^2\left(\nabla^2\big(W(x,y)\big)\right) \tag{12}$$

where $\nabla^2 = \partial^2/\partial x^2 + \partial^2/\partial y^2$ is the Laplace operator. In Eq. (12), $\nabla^2\big(W(x,y)\big)$ is first estimated according to a bivariate polynomial in the form of

$$\widehat{W}_p(x,y) = c_{2,0}x^2 + c_{1,1}xy + c_{0,2}y^2 + c_{1,0}x + c_{0,1}y + c_{0,0} \tag{13}$$

Then, $\nabla^2\big(W(x,y)\big)$ is fitted using the same form of the bivariate polynomial as shown in Eq. (13) to evaluate $\nabla^4\big(W(x,y)\big)$.

In the proposed procedure, the selection of the number of local measurement points for polynomial fitting plays a vital role in determining the noise-robustness and estimate accuracy of $\nabla^4\big(W(x,y)\big)$, which subsequently affects the damage localization. Here, in order to better represent the number of local measurement points, rings around a centre point are used, as shown in Fig.1. Theoretically, the more rings are used in the fitting, the more noise-robust and smooth the estimated spatial derivatives of $W(x,y)$ are, but the less sensitive to damage-induced local features. Therefore, an appropriate selection of the number of rings N_p is required to obtain the most accurate damage localization. To simplify the selection of N_p, the double fitting process based on Eq. (13) using the same N_p is constructed. Moreover, an automatic approach for adjusting N_p for obtaining the best damage localization performance will be presented in detail in the next section.

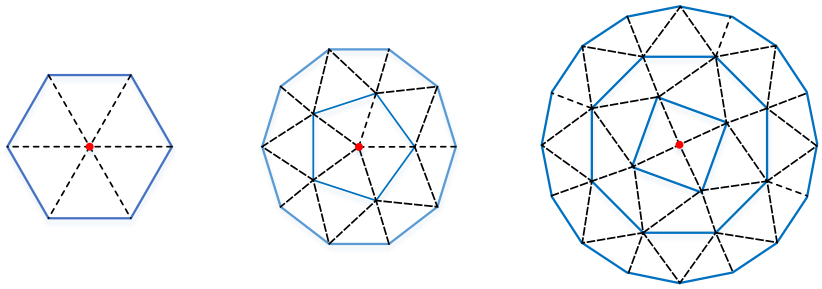

（a） （b） （c）

Figure 1. Adjacent measurement points: (a) 1 ring, (b) 2 rings and (c) 3 rings.

4.2 Adaptive determination of N_p via hierarchical clustering

A typical demonstration of the elements of $DI(x,y)$ under a multi-damage scenario is graphed in Fig.2. Usually, the outlier values due to local damage tend to be close to each other whilst the noise-caused outlier values are scattered over the 2-D plate surface. A smaller N_p can hardly suppress the effects of measurement noise, thus leading to a poor damage localization. By increasing N_p, fine-scale features would gradually disappear, which include both the noise effects and damage-induced local features. Therefore, an appropriate selection of N_p is essential to accurately localize the damage zones whilst suppressing the noise effects.

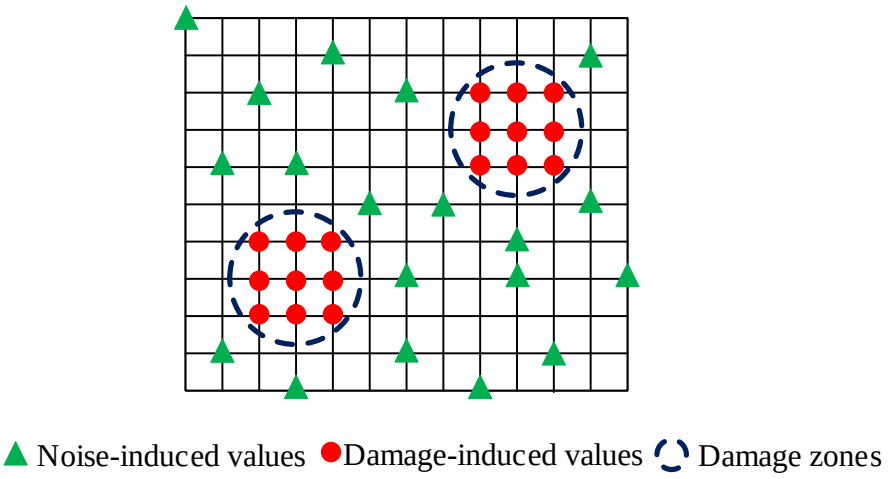

Figure 2. Illustration of outlier values of $DI(x,y)$.

To determine the optimal N_p, a hierarchical clustering approach is proposed, which measures the dissimilarity between the sets of outlier values. In this approach, a single-linkage clustering is adopted

to evaluate the shortest distance that involves all the outlier values of $DI(x,y)$, which is depicted in Fig. 3. The links between outlier values are represented as upside-down U-shaped lines. The height of the U indicates the distance between outlier values. For example, the link representing cluster 1 contains a large number of outlier values due to a damage, which are spatially close to each other, whereas the clusters due to measurement noise have a large distance to each other and each cluster contains just one or two outlier values. Therefore, the number of clusters due to measurement noise as described in Fig. 3 is a performance indicator of damage localization. Normally, the fewer the noise-induced clusters, the more noise-robust and accurate the damage localization results.

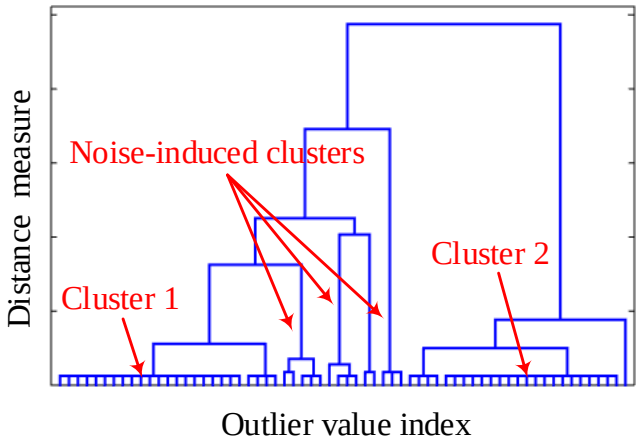

Figure 3. Illustration of hierarchical clustering dendrogram of $DI(x,y)$.

Furthermore, the number of clusters N_c associated with the measurement noise decreases gradually by increasing N_p, as the outlier values due to measurement noise are smoothened when a larger N_p is used. Therefore, the selection of N_p can be determined by the calculation of N_c. To calculate N_c, the proposed steps are summarized as follows:

Step 1: Compute the dissimilarity between each pair of outlier values in $DI(x,y)$. For instance, with (x_k, y_k) and (x_l, y_l) representing the coordinates of two outlier values, the dissimilarity is evaluated by using Euclidean distance as

$$d_{kl} = \sqrt{(x_k - x_l)^2 + (y_k - y_l)^2} \tag{14}$$

Sep 2: Group the outlier values into a cluster tree as shown in Fig. 3. The outlier values are linked in close proximity using the single-linkage criterion. Mathematically, the single-linkage criterion is expressed as

$$d(R,S) = \min_{r \in R, s \in S} d(r,s) \quad (15)$$

where R and S denote any two sets of elements considered as clusters, and $d(r,s)$ indicates the distance between two elements r and s.

Step 3: Identify and sum up the number of the clusters N_c that contain one or two outlier values, which are considered corresponding to the measurement noise as demonstrated in Fig. 3.

To avoid possible over-smoothing of the damage-induced local features, the lowest number N_p of fitting rings that makes N_c zero will be chosen for damage localization.

5 Numerical studies

Cantilever aluminium plates of dimension $0.35 \times 0.23 \times 0.003\text{m}^3$ with Young's modulus E=69 GPa, Poisson's ratio $\nu = 0.35$ and mass density ρ=2700 kg/m^3 are studied. Based on the Mindlin plate theory, the plates are modelled in MATLAB by using the four-node quadrilateral shell elements. Here, the use of Mindlin plate theory would allow the re-examination of the possible shear and rotational effects of the plates on the validity of the proposed methodology based on Kirchoff-Love theory. For numerical integration, 2×2 Gauss points are used for the bending contribution and 1 Gauss point is used for the shear contribution, which are proved to be one of the simplest approach to avoid shear locking [38].

The plates are clamped on the left and discretized into 140×92 equal-sized elements of $0.0025 \times 0.0025 \times 0.003\text{m}^3$. Two damage scenarios are studied and the damage is introduced by reducing the thickness of the associated FE elements, as shown in Fig. 4. In numerical case 1, two damage zones are centred at (0.10m, 0.115m) and (0.21m, 0.115m) with an equal area of 0.02×0.02 m^2. For numerical case 2, two damage zones are centred at (0.155 m, 0.075 m) and (0.155 m, 0.155 m) with the same equal area of 0.02×0.02 m^2. In both damage scenarios, the damage zones of the plate thickness are reduced by 5% with respect to the pristine plate.

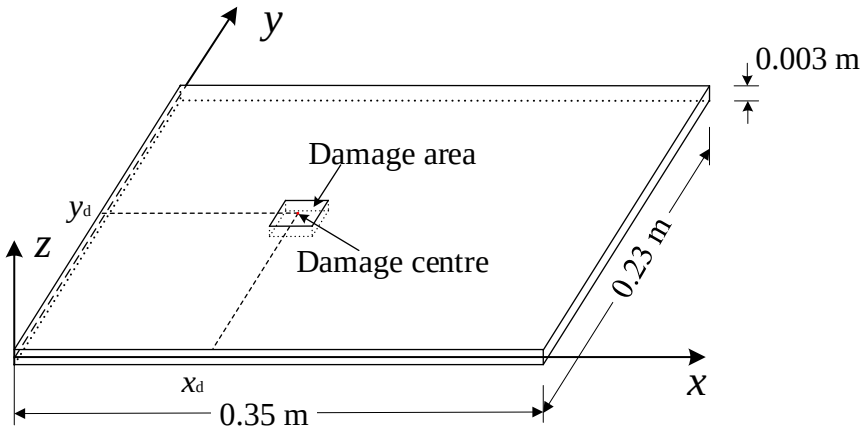

Figure 4. Configuration of a plate with damage.

The purposes of numerical studies are twofold. First, at a single angular frequency, the proposed adaptive damage localization method will be proved to be noise-robust and effective for damage localization under noisy condition. Secondly, the enhanced PE method that integrates damage information at several angular frequencies will be demonstrated to be more effective and robust for damage localization.

5.1 Verification of the proposed adaptive damage localization

In this section, the 10th mode, shown in Fig. 5, which is sensitive to the two damage zones of numerical case 1, is first investigated to verify the feasibility and the effectiveness of the proposed adaptive damage localization method. Then, the 10th mode is shown to be ineffective for numerical case 2 and hence the combination of damage-induced features of more than one mode proved to be necessary for robust damage localization.

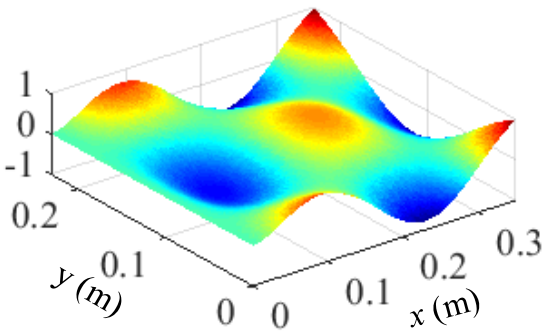

Figure 5. The 10th mode shape.

The damage localization results in numerical case 1 without and with noise are presented in Figs. 6 (a) and (b), respectively. For the noisy case, a Gaussian white noise of SNR=60dB (SNR represents the signal to noise ratio) is added.

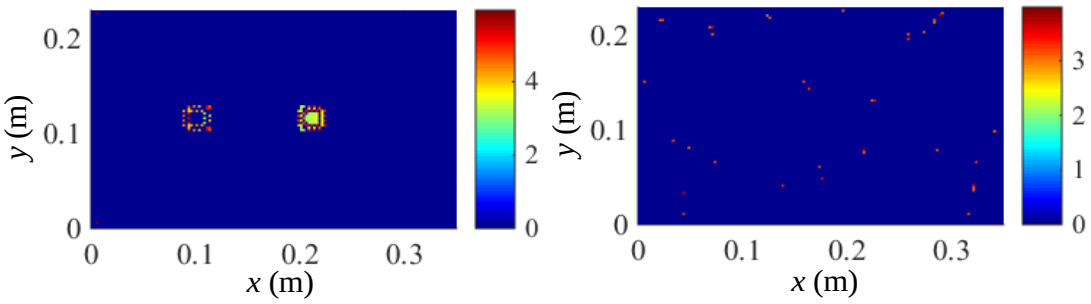

(a) (b)

Figure 6. $|DI(x,y)|$ of the 10th mode shape for numerical case 1: (a) without noise effects and (b) with SNR= 60dB.

It is seen from Fig. 6(a) that the damage index $DI(x,y)$ of the original PE method is able to accurately localize the two damage zones. However, the localization results are severely degraded by the presence of measurement noise as shown in Fig. 6(b). Moreover, the noise-induced outlier values of $DI(x,y)$ in Fig. 6(b) are scattered over the plate surface and are rarely close to each other. Therefore, the proposed approach of quantifying the noise-induced characteristics of $DI(x,y)$ in Section 4.2 is reasonable.

Next, for the noisy case in Fig. 6(b), the proposed adaptive fourth-order derivative estimation approach is applied and the number of the fitting rings N_p is optimized as shown in Fig. 7.

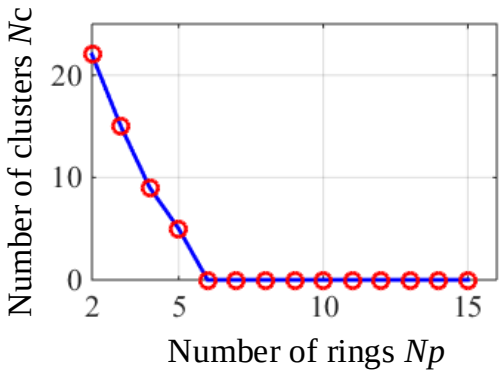

Figure 7. N_c at different N_p for numerical case 1.

It can be seen that the noise-induced clusters N_c decreases rapidly when N_p increases. N_p=6 is automatically determined, as the corresponding N_c first reduces to zero. Damage localization results using different N_p= 2, 6, 10, 14 are presented in Fig. 8. The actual positions of the damage zones are indicated by white boxes.

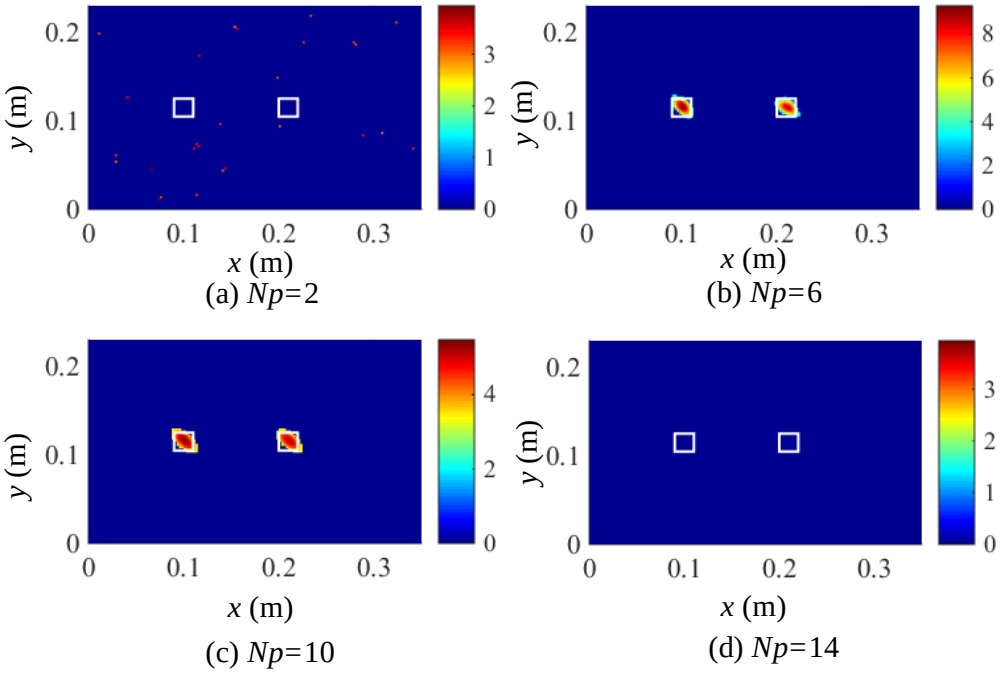

Figure 8. Damage localization results when using different N_p for numerical case 1.

By comparing Fig. 8(a) with Fig. 8(b), it is apparent that the effects of measurement noise are significantly reduced and the two damage zones are accurately identified when using N_p=6. In Fig. 8 (c), N_p is further increased to 10 and the damage localization results indicate that a larger N_p is able to enlarge the detected damage areas. Finally, at N_p=14 as shown in Fig. 8(d), the damage-induced local characteristics are totally smoothened. These observations confirm the fact that a proper selection of N_p is indeed essential for accurate damage localization. Moreover, the proposed adaptive selection procedure for N_p is an effective way to obtain accurate damage localization results.

Then, the 10th mode is used to localize the two damage zones of numerical case 2. First, the damage localization results with and without noise are graphed in Fig. 9. Figure 9(a) shows that the two damage zones cannot be effectively localized by using the 10th mode shape. Furthermore, the presence of the measurement noise severely degrades the localization results, as shown in Fig. 9(b). After this,

the proposed adaptive damage localization is applied and the obtained damage localization results are illustrated in Fig. 10. It indicates that the noise-induced clusters decreasing to zero is achieved when N_p=7 and the damage-induced local characteristics are clearly manifested. However, this mode is not effective for detecting these two particular damage zones. As expected, a single mode or operational deflection shape at a certain angular frequency may not lead to the desirable robustness for damage localization.

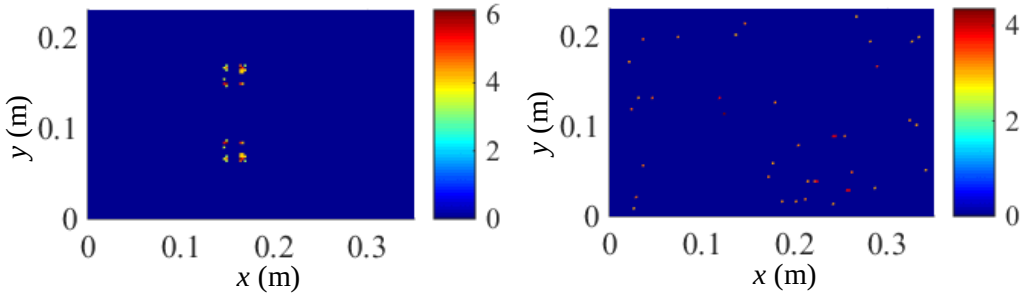

(a) (b)

Figure 9. $|DI(x,y)|$ by using the 10th mode for numerical case 2: (a) without noise effects and (b) with SNR= 60dB.

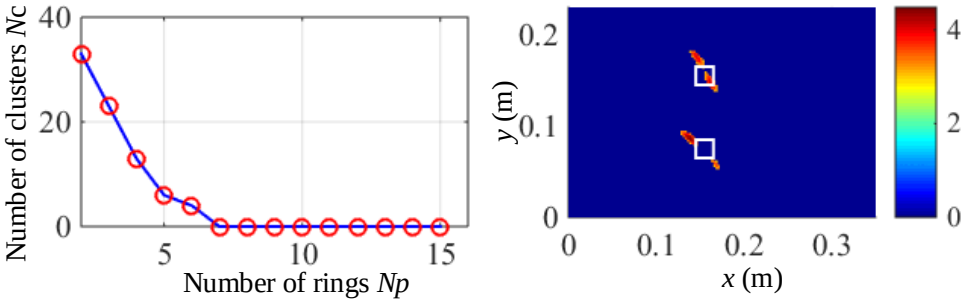

(a) N_c under different N_p (b) N_p=7

Figure 10. (a) Noise-induced clusters at different N_p and (b) Damage localization results when using N_p=7 for numerical case 2.

Finally, the sensitivity of the proposed method to the number of measurement points is investigated using numerical case 1. Localization results are presented in Fig.11. It can be seen that by gradually reducing the measurement point number to a certain extent, down to 36×29, the identified damage shapes become coarse, but still detectable. However, a further reduced grid, *e.g.* 18×15, is obviously not enough. Therefore, sufficient measurement points are required to ensure the detectability.

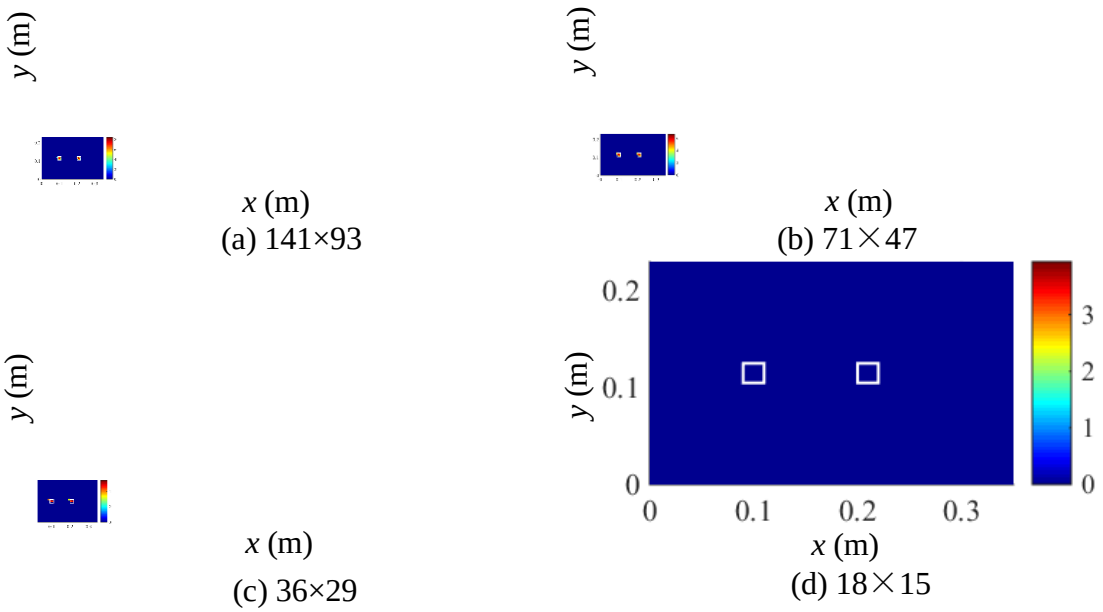

Figure 11. Damage localization results on numerical case 1 based on the 10th mode shape using different measurement points.

5.2 Enhanced adaptive damage localization index

To obtain a robust damage localization results, the proposed integrated $DI(x,y)$ as defined in Eq. (7) is applied. Here, the 1st to 5th modes (lower modes) and the 10th to 15th modes (higher modes) contaminated by a Gaussian white noise of SNR=60dB are used to show the effectiveness of the proposed integrated $DI(x,y)$. Localization results are depicted in Fig. 12 and Fig. 13, respectively. It can be seen that the two damage zones can be accurately localized in both damage scenarios by using combinations of lower modes and higher modes. However, comparisons between Fig. 12 and Fig. 13 suggest that higher modes tend to provide more accurate damage localization results, as expected. For practical applications, with the damage information unknown *a priori*, it is better to combine all the available modes for a more robust damage localization.

(a) (b)

Figure 12. Integrated damage localization by using the first five mode shapes: (a) Numerical case 1 and (b)Numerical case 2.

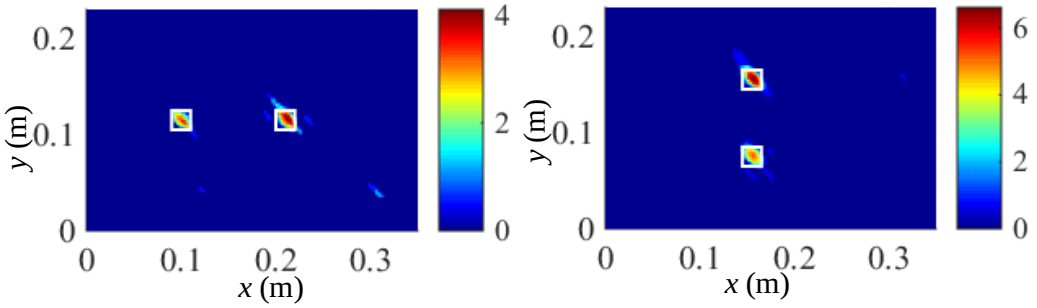

(a) (b)

Figure 13. Integrated damage localization by using the 10th to 15th modes: (a) Numerical case 1 and (b) Numerical case 2.

6 Experimental studies

As experimental validation, two cantilever aluminium plates with the same geometrical properties as those used in the numerical study are fabricated and tested. The experiment set-up is shown in Fig. 14.

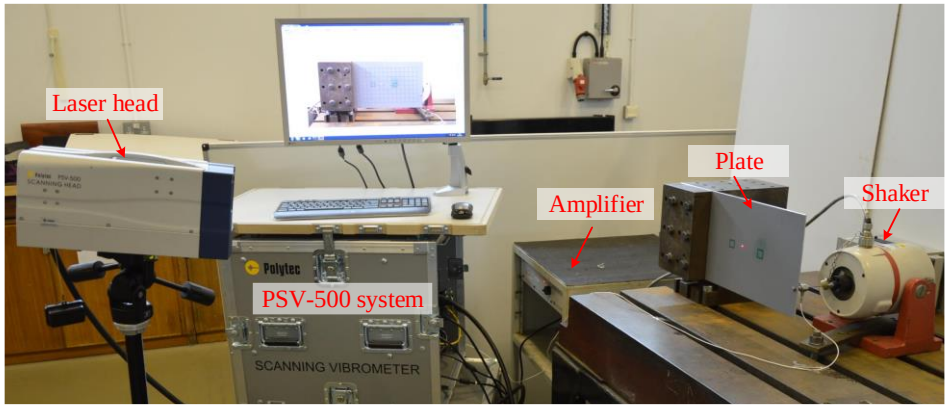

Figure 14. Experiment set-up of testing a cantilever plate.

The damage is introduced by reducing 10% of the plate thickness on the opposite side of the measurement surface. Other parameters of the two studied damage cases are manufactured according to the two damage scenarios of the numerical study. The plates are clamped on the left and excited by a shaker (LDS V406) on the right. Vibration responses are measured by a scanning laser vibrometer (PSV-500 SLV) under sinusoidal excitation. First, a pseudo random excitation signal of 0-2000 Hz is applied to search for the resonant frequencies of the plate. The sampling rate is 5000Hz. Then, the 'FastScan' mode is adopted. By setting a specific excitation frequency of interest, excitation signal feeds an electromechanical shaker, producing an excitation force with an amplitude of 5N.

For case 1, 141×95 measurement points are assigned, which span from 0.0084m to 0.3334m in the x direction and 0.0028m to 0.2218m in the y direction. For case 2, the measurement zone slightly differs from experimental case 1 but 141×95 measurement points are still used. During the experiments, 30 averages are taken for each measurement point, resulting in a total measurement time of 30 minutes for 141 × 95 measurement points.

Firstly, the 10th mode is used as a representative and the proposed damage index based on the central difference method for the fourth-order derivative estimation is used to identify the two damage zones in both experimental cases, with damage localization results shown in Fig. 15. The actual positions of the damage zones are indicated by white boxes. Figure 15 demonstrates that without using denoising techniques, the traditional PE method is barely capable of detecting the damage.

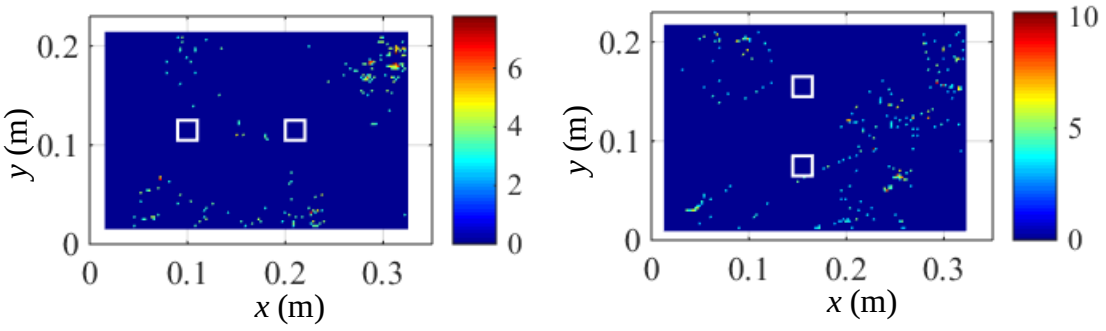

(a) (b)

Figure 15. Damage localization of the traditional PE method: (a) Experimental case 1 and (b) Experimental case 2.

Then, the proposed adaptive damage localization method is used and the damage localization results

of the two experimental damage cases are illustrated in Fig. 16 and Fig. 17, respectively. From Fig. 16, one concludes that the proposed adaptive damage localization approach is effective in reducing the noise effects and providing accurate damage localization results. Moreover, the denoising capability of the proposed method is further validated in Fig. 17 but only one damage zone is detected. Therefore, the damage-induced local features at a single frequency is not robust for damage localization and the damage information at more frequencies should be incorporated to provide an accurate and robust damage localization.

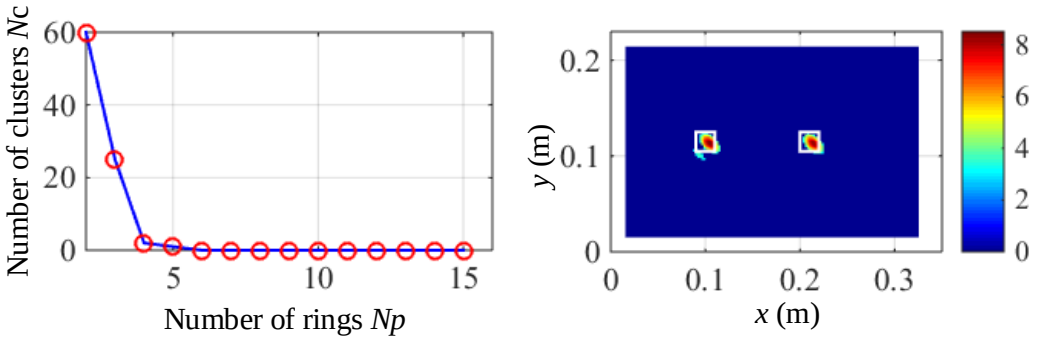

(a) N_c under different N_p (b) N_p=6

Figure 16. (a) Noise-induced clusters at different N_p and (b) Damage localization results when using N_p=6 for experimental case 1.

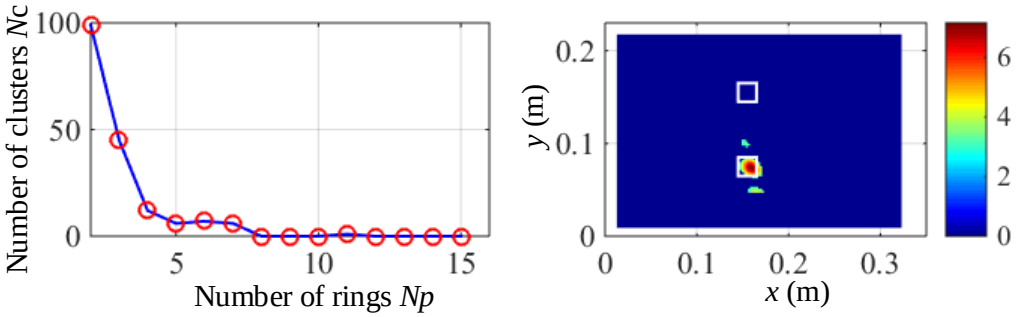

(a) N_c under different N_p (b) N_p=8

Figure 17. (a) Noise-induced clusters at different N_p and (b) Damage localization results when using N_p=8 for experimental case 2.

To demonstrate the proposed integrated $DI(x,y)$ in Eq. (7), the 10th and 13th modes are used with results for the two experimental cases presented in Fig. 18, which would be shown to be sufficient and efficient. It is clear that the two damage zones in both experimental cases are accurately localized. Therefore, in practical applications with the damage information unknown *a priori*, mode shapes or

operational deflection shapes at different angular frequencies should be combined in the proposed adaptive damage localization method to avoid blind inspection zones.

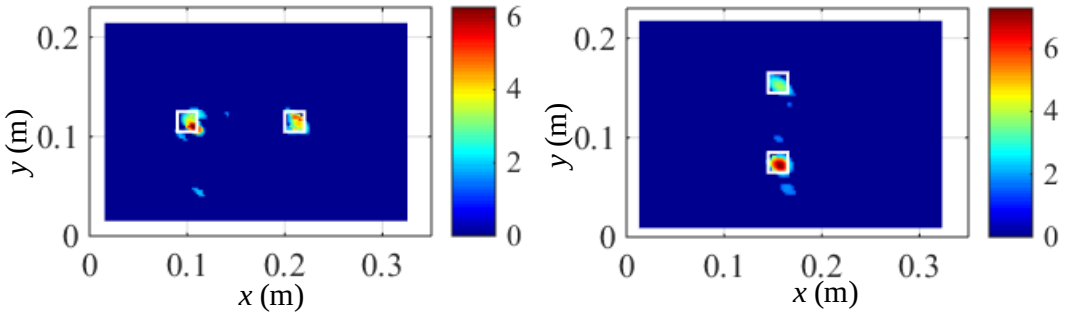

Figure 18. Integrated damage localization results: (a) Experimental case 1 and (b) Experimental case 2.

7 Conclusions

A novel adaptive multi-damage localization method, based on a local vibration model and hierarchical clustering, is proposed. Compared with the traditional high-order spatial derivative-based damage localization methods, the proposed method optimizes the process for the high-order spatial derivative estimation to achieve more accurate damage localization. Moreover, the damage index is constructed based on an identified general local vibration model of the inspected structures with unknown material/structural parameters, under the assumption that damage only occupies a small area of the inspected structural component and the rest of the inspected structure still satisfies the local vibration model in the absence of any external excitation. Owing to these features, the method can be implemented for structures without baseline data and the information on material/structural properties. As part of the method, an enhanced damage localization index is proposed by integrating the damage-induced features in modes or more generally, structural characteristic deflection shapes at different angular frequencies. Numerical and experimental studies on two plates with two damage zones are conducted to demonstrate the improved performance of the proposed adaptive damage localization method.

Several major conclusions are summarized as follows:

1. The quantification of the local dynamic equilibrium is an effective approach for damage

localization, even when some material/structural properties are unknown *a priori*. By incorporating the damping effects into the model, the applicability of the traditional PE method is extended to resonant conditions. Furthermore, a statistical thresholding approach is proposed to enhance the noise-robustness of the defined damage localization index.

2. Hierarchical clustering is shown to be an effective tool for noise feature quantification and the improvement of the damage localization accuracy. A fully automatic framework to obtain the most accurate damage localization is developed based on hierarchical clustering. Firstly, the noise-induced features in the damage index are quantified via hierarchical clustering. Then, the noise effects on the damage index are reduced to a minimal level by tuning the process of spatial derivative estimation.

3. A robust damage localization approach should integrate the damage information from multiple modes or operational deflection shapes at different frequencies, to avoid the blind inspection area that each one may have.

Acknowledgements

This work was partially supported by a grant from the Innovation and Technology Commission of the HKSAR Government to the Hong Kong Branch of National Rail Transit Electrification and Automation Engineering Technology Research Centre. The experiments were carried out in the School of Engineering, University of Liverpool.

References

[1] Y. Yan, L. Cheng, Z. Wu, L. Yam, Development in vibration-based structural damage detection technique, Mechanical Systems and Signal Processing, 21 (2007) 2198-2211.
[2] D. Montalvao, N.M.M. Maia, A.M.R. Ribeiro, A review of vibration-based structural health monitoring with special emphasis on composite materials, Shock and Vibration Digest, 38 (2006) 295-326.
[3] G.R. Gillich, H. Furdui, M.A. Wahab, Z.I. Korka, A robust damage detection method based on multi-modal analysis in variable temperature conditions, Mechanical Systems and Signal Processing, 115 (2019) 361-379.
[4] J.E. Mottershead, M. Link, M.I. Friswell, The sensitivity method in finite element model updating: a tutorial, Mechanical Systems and Signal Processing, 25 (2011) 2275-2296.
[5] J. Xiang, T. Matsumoto, Y. Wang, Z. Jiang, Detect damages in conical shells using curvature mode

shape and wavelet finite element method, International Journal of Mechanical Sciences, 66 (2013) 83-93.
[6] V. Morovati, M. Kazemi, Detection of sudden structural damage using blind source separation and time–frequency approaches, Smart Materials and Structures, 25 (2016) 055008.
[7] S. Cao, H. Ouyang, Robust structural damage detection and localization based on joint approximate diagonalization technique in frequency domain, Smart Materials and Structures, 26 (2017) 015005.
[8] C. Surace, R. Saxena, M. Gherlone, H. Darwich, Damage localisation in plate like-structures using the two-dimensional polynomial annihilation edge detection method, Journal of Sound and Vibration, 333 (2014) 5412-5426.
[9] M. Krishnan, B. Bhowmik, A. Tiwari, B. Hazra, Online damage detection using recursive principal component analysis and recursive condition indicators, Smart Materials and Structures, 26 (2017) 085017.
[10] S.W. Doebling, C.R. Farrar, M.B. Prime, A summary review of vibration-based damage identification methods, Shock and Vibration Digest, 30 (1998) 91-105.
[11] J.K. Sinha, M. Friswell, S. Edwards, Simplified models for the location of cracks in beam structures using measured vibration data, Journal of Sound and Vibration, 251 (2002) 13-38.
[12] K. Worden, J.M. Dulieu-Barton, An overview of intelligent fault detection in systems and structures, Structural Health Monitoring, 3 (2004) 85-98.
[13] K. Mendrok, T. Uhl, Experimental verification of the damage localization procedure based on modal filtering, Structural Health Monitoring, 10 (2011) 157-171.
[14] M.M.A. Wahab, G. De Roeck, Damage detection in bridges using modal curvatures: application to a real damage scenario, Journal of Sound and Vibration, 226 (1999) 217-235.
[15] M. Thiene, M. Zaccariotto, U. Galvanetto, Application of proper orthogonal decomposition to damage detection in homogeneous plates and composite beams, Journal of Engineering Mechanics, 139 (2013) 1539-1550.
[16] H. Xu, L. Cheng, Z. Su, J.L. Guyader, Identification of structural damage based on locally perturbed dynamic equilibrium with an application to beam component, Journal of Sound and Vibration, 330 (2011) 5963-5981.
[17] H. Xu, B. Lu, Z. Su, L. Cheng, Statistical enhancement of a dynamic equilibrium-based damage identification strategy: Theory and experimental validation, Journal of Sound and Vibration, 351 (2015) 236-250.
[18] C. Pezerat, J. Guyader, Identification of vibration sources, Applied acoustics, 61 (2000) 309-324.
[19] A. Berry, O. Robin, F. Pierron, Identification of dynamic loading on a bending plate using the Virtual Fields Method, Journal of Sound and Vibration, 333 (2014) 7151-7164.
[20] J. Sanchez, H. Benaroya, Review of force reconstruction techniques, Journal of Sound and Vibration, 333 (2014) 2999-3018.
[21] Q. Leclère, F. Ablitzer, C. Pézerat, Practical implementation of the corrected force analysis technique to identify the structural parameter and load distributions, Journal of Sound and Vibration, 351 (2015) 106-118.
[22] M.L. Fugate, H. Sohn, C.R. Farrar, Vibration-based damage detection using statistical process control, Mechanical Systems and Signal Processing, 15 (2001) 707-721.
[23] M. Cao, P. Qiao, Integrated wavelet transform and its application to vibration mode shapes for

the damage detection of beam-type structures, Smart Materials and Structures, 17 (2008) 055014.
[24] Y. Shokrani, V.K. Dertimanis, E.N. Chatzi, M. N. Savoia, On the use of mode shape curvatures for damage localization under varying environmental conditions, Structural Control and Health Monitoring, 25 (2018) e2132.
[25] H. Xu, Z. Su, L. Cheng, J.L. Guyader, P. Hamelin, Reconstructing interfacial force distribution for identification of multi-debonding in steel-reinforced concrete structures using noncontact laser vibrometry, Structural Health Monitoring, 12 (2013) 507-521.
[26] H. Xu, L. Cheng, Z. Su, Suppressing influence of measurement noise on vibration-based damage detection involving higher-order derivatives, Advances in Structural Engineering, 16 (2013) 233-244.
[27] Y. Xu, D. Chen, W. Zhu, Damage identification of beam structures using free response shapes obtained by use of a continuously scanning laser doppler vibrometer system, Mechanical Systems and Signal Processing, 92 (2017) 226-247.
[28] P. Moreno-García, H. Lopes, J.A. dos Santos, Application of higher order finite differences to damage localization in laminated composite plates, Composite Structures, 156 (2016) 385-392.
[29] W. Xu, M. Radzieński, W. Ostachowicz, M. Cao, Damage detection in plates using two-dimensional directional Gaussian wavelets and laser scanned operating deflection shapes, Structural Health Monitoring, 12 (2013) 457-468.
[30] M. Cao, Z. Su, L. Cheng, H. Xu, A multi-scale pseudo-force model for characterization of damage in beam components with unknown material and structural parameters, Journal of Sound and Vibration, 332 (2013) 5566-5583.
[31] M. Cao, L. Cheng, Z. Su, H. Xu, A multi-scale pseudo-force model in wavelet domain for identification of damage in structural components, Mechanical Systems and Signal Processing, 28 (2012) 638-659.
[32] W. Xu, M.S. Cao, W. Ostachowicz, M. Radzieński, N. Xia, Two-dimensional curvature mode shape method based on wavelets and Teager energy for damage detection in plates, Journal of Sound and Vibration, 347 (2015) 266-278.
[33] Z. Yang, M. Radzienski, P. Kudela, W. Ostachowicz, Two-dimensional modal curvature estimation via Fourier spectral method for damage detection, Composite Structures, 148 (2016) 155-167.
[34] H. Xu, Q. Zhou, M. Cao, Z. Su, Z. Wu, A dynamic equilibrium-based damage identification method free of structural baseline parameters: experimental validation in a two-dimensional plane structure, Journal of Aerospace Engineering, 31 (2018) 04018081.
[35] S. Cao, H. Ouyang, L. Cheng, Baseline-free adaptive damage localization of plate-type structures by using robust PCA and Gaussian smoothing, Mechanical Systems and Signal Processing, 122 (2019) 232-246.
[36] M. Meyer, M. Desbrun, P. Schröder, A.H. Barr, Discrete differential-geometry operators for triangulated 2-manifolds, Visualization and mathematics, 3 (2002) 52-58.
[37] J. Goldfeather, V. Interrante, A novel cubic-order algorithm for approximating principal direction vectors, ACM Transactions on Graphics (TOG), 23 (2004) 45-63.
[38] A.J.M. Ferreira, MATLAB codes for finite element analysis: solids and structures, Springer Science & Business Media, 2008.